# Simulation of fracture on PFRC specimens subjected to high temperature using a cohesive model

F. Suárez
*Departamento de Ingeniería Mecánica y Minera*
*Universidad de Jaén, Jaén, Spain.*

A. Enfedaque & M.G. Alberti & J.C. Gálvez
*Departamento de Ingeniería Civil: Construcción, E.T.S de Ingenieros de Caminos, Canales y Puertos*
*Universidad Politécnica de Madrid, Madrid, Spain.*

ABSTRACT: Concrete has been traditionally reinforced with steel rebars that confer good tensile properties to this material. Nevertheless, concrete can also be reinforced with fibres, which have been traditionally made of steel, although in the last years new types of fibres have appeared, such as polypropylene fibres, glass fibres or polyolefin fibres. Their use widens the range of application of fibre-reinforced concrete (FRC) and has experienced an significant boost by national and international standards, which now include guidelines for their use in structures. More specifically, textured polyolefin macro-fibres have proved to provide very good tensile properties in concrete. The use of these fibres has significant advantages when compared with traditional steel fibres, since they reduce the tear and wear of devices involved in their production, avoid corrosion problems in concrete and have no influence on magnetic fields, which can be very important in some situations. Concrete properties, both in fresh and hardened states, have been extensively studied in the last years, proving to be a promising alternative to steel fibres. Fracture of FRC, and more specifically of PFRC, has been successfully reproduced using the finite element analysis by means of an embedded cohesive model with a trilinear softening function. On another note, concrete has a good behaviour when subjected to high temperatures and fire, especially when it is compared with other traditional construction materials, such as wood or steel. Nevertheless, concrete reinforcement is usually made of materials that are critically sensitive to these events and the behaviour of the composite material must be assessed to meet the requirements described in the structural standards. With regard to polyolefin-fibre reinforced concrete (PFRC), a recent study has analysed how the fracture properties of this material degrade when subjected to high-temperatures, ranging from 20ºC to 200ºC. As temperature increases, fibres modify their geometry and their mechanical properties, which leads to a reduction of their effectiveness. In this work, the fracture behaviour of PFRC specimens subjected to high temperatures is reproduced by using an embedded cohesive model that uses a trilinear softening function. The specific trilinear softening diagram that provides a good numerical simulation of fracture is obtained for each temperature increment. This helps to understand how the trilinear diagram must be adapted when PFRC is subjected to high temperatures and will allow the use of this model to a wider range of situations.

## 1 INTRODUCTION

The use of reinforced concrete (RC) in the confinement of nuclear reactors boasted the studies regarding the fire resistance of concrete in the last decades of the last century (Bažant & Kaplan 1996). In such studies it was evident that, not only the resistance of concrete was essential, but also the properties of the reinforcing steel that was used to enhance the flexural and tensile strength of RC. Analogously, when fibres are added to concrete forming fibre reinforced concrete (FRC) the response of fibres to high temperatures influences the fire resistance of the material. Such influence might be beneficial as in the case of polypropylene fibres (PF). Using PF fibres in determined dosages has proved to reduce the risk of explosive spalling in concrete (Varona, Baeza, Bru, & Ivorra 2018a, Liu, Ye, De Schutter, Yuan, & Taerwe 2008). PF fibres melt when subjected to high temperatures and generate a capillary network that reduces the high pressures preventing the spalling of the concrete element. However, the contribution of the PF to the structural behaviour of the concrete element cannot be considered due to its reduced

mechanical properties.

Steel fibres (SF) have been traditionally employed in structural applications obtaining successful results (Lopez, Serna, Camacho, Coll, & Navarro-Gregori 2014). Moreover, if certain requirements are met, some standards and recommendations enable to reduce, or even substitute, the steel reinforcing bars of the concrete element. However, structural elements manufactured with steel fibre reinforced concrete (SFRC) exhibits explosive spalling no matter the dosage of steel fibres used. Cocktails of fibres, obtained by mixing SF and PP, have been successfully applied in elements where not only the mechanical behaviour has been improved but also its fire resistance (Varona, Baeza, Bru, & Ivorra 2018a, Yermak, Pliya, Beaucour, Simon, & Noumowé 2017, Varona, Baeza, Bru, & Ivorra 2018b). Moreover, it should be mentioned that several authors have devoted studies to model the constitutive behaviour of SFRC when subjected to high temperatures (Ruano, Isla, Luccioni, Zerbino, & Giaccio 2018, Moradi, Bagherieh, & Esfahani 2020, Abdallah, Fan, & Cashell 2017). The existence of these models is of importance as they might help to estimate the residual load bearing capacity of the material and consequently the reliability of the structural elements after being subjected to high temperatures.

The appearance of polyolefin macro fibres with structural capacities have shown their suitability for their use in structural elements when added to concrete forming polyolefin fibre reinforced concrete (PFRC) (Alberti, Enfedaque, & Gálvez 2015, Alberti, Enfedaque, Gálvez, & Pinillos 2017, Picazo, Gálvez, Alberti, & Enfedaque 2018). In addition, there are recent studies that have analysed the influence of high temperatures in the mechanical behaviour of PFRC (Alberti, Gálvez, Enfedaque, & Castellanos 2021). However, there are not numerous studies concerning the changes that temperature generates in the constitutive models used in the structural design of PFRC structural elements.

Among all the mechanical properties of PFRC, the one that determines the structural character of the material is the fracture behaviour when subjected to flexural stresses. Due to this, significant effort has been recently devoted to find constitutive models that reproduce the flexural fracture behaviour of PFRC. One of the most successful attempts has been carried out by using a cohesive crack approach and an inverse analysis. Merging both concepts, the material behaviour obtained in experimental tests has been reproduced. It has been shown that the trilinear softening functions implemented were capable of considering the dosage of fibres (Alberti, Enfedaque, Gálvez, & Reyes 2017), their orientation (Enfedaque, Alberti, & Gálvez 2019) or even the size effect (Suárez, Gálvez, Alberti, & Enfedaque 2021). Moreover, they were apt also for simulating the behaviour of the material when subjected to tensile streses (Enfedaque, Alberti, Galvez, & Beltran 2018) or a combination of flexural-shear stresses (Suárez, Gálvez, Enfedaque, & Alberti 2019).

Based on the results shown in (Alberti, Gálvez, Enfedaque, & Castellanos 2021) this contribution seeks to determine the changes that should be performed in the constitutive model of PFRC when subjected to a flexural fracture test after being exposed to a range of temperature from 20 °C to 200 °C. Although in the referred work two PFRC mixes were analysed, with 3 kg of fibres per $m^3$ (HF3) and with 10 kg of fibres per $m^3$ (HF10), here only the results of the first of them are numerically reproduced.

## 2 EXPERIMENTAL BENCHMARCK

The experimental campaign was carried with specimens manufactured by using the concrete formulations and procedures described in (Alberti 2015). Portland cement type EN-197-1 CEM I 52.5 R-SR and Sika Viscocrete 5720, a policarboxylic superplastisicer, were mixed with siliceous aggregates (12.7 mm of maximum size). In addition, a limestone powder with a content of content of 98% calcium carbonate was employed. The mix formulation can be seen in Table 1.

Table 1: Mix proportions used concrete in the experimental campaign (Alberti, Gálvez, Enfedaque, & Castellanos 2021).

| | HF | HF3 | HF10 |
|---|---|---|---|
| Cement ($kg/m^3$) | 375 | 375 | 375 |
| Limestone powder ($kg/m^3$) | 100 | 100 | 100 |
| Water ($kg/m^3$) | 187.5 | 187.5 | 187.5 |
| Sand ($kg/m^3$) | 916 | 916 | 916 |
| Gravel ($kg/m^3$) | 300 | 300 | 300 |
| Grit ($kg/m^3$) | 450 | 450 | 450 |
| Superplasticiser (% cement weight) | 0.75 | 0.75 | 0.75 |
| Polyolefin fibres ($kg/m^3$) | - | 3 | 10 |

In the formulations with fibres 60 mm-long polyolefin fibres were added. Such fibres have a superficial treatment and embossed surface in order to provide a proper response of the fibre-matrix interface.

The outlook of the fibres can be seen in Figure 2. Besides, the most representative properties of the fibres can be seen in Table 2.

Figure 1: Appearance of the fibres used (scale in mm).

Table 2: Fibre properties and dimensions.

| | |
|---|---|
| Density ($g/cm^3$) | 0.91 |
| Length (mm) | 60 |
| Eq. diameter (mm) | 0.92 |
| Tensile strength (MPa) | >500 |
| Modulus of elasticity (GPa) | >9 |

The specimens were heated in a convection oven at an approximate heating rate of 2.80 °C/min. The specimens remained at the chosen temperature for 3 hours after being cooled progressively during 7 hours inside the oven. The flexural tests were performed after the cooling period. The characterisation of the concrete elements was performed considering three temperatures as reference: room temperature, 150ºC and 200ºC. The latter two temperatures correspond to a temperature at which the fibres still maintained some integrity and a temperature at which the fibres were remarkably damaged respectively. In order to determine the influence of temperature in a PFRC formulation that was considered as a structural material (HF10) several increments of temperature were chosen between 150ºC and 200ºC.

The flexural fracture behaviour of the material was determined following the standard RILEM TC-187-SOC (Planas, Guinea, Gálvez, Sanz, & Fathy 2007). The test setup can be seen in Figure 1.

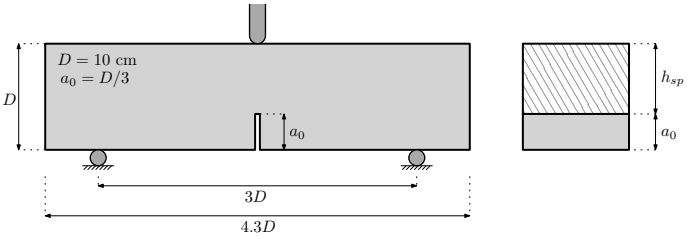


Figure 2: Scheme of the three-point bending test used in (Planas, Guinea, Gálvez, Sanz, & Fathy 2007).

As can be observed in Figure 2, the notch length was equal to $D/3$ and the span between the bearing cylinders was equal to $3D$. In this figure, $a_0$ corresponds to the notch length, $h_{sp}$ to the ligament length and $P$ to the applied load. The test data was acquired by means of two Linear Variable Differential Transformer (LVDT) placed at each side of the specimens and a Crack Mouth Opening Displacement (CMOD) mounted in the lips of the notch. In addition, the load borne by the sample, the position of the actuator and the elapsed time were also recorded.

In Figure 3 the average load-deflection curves obtained in the tests can be seen.

a)

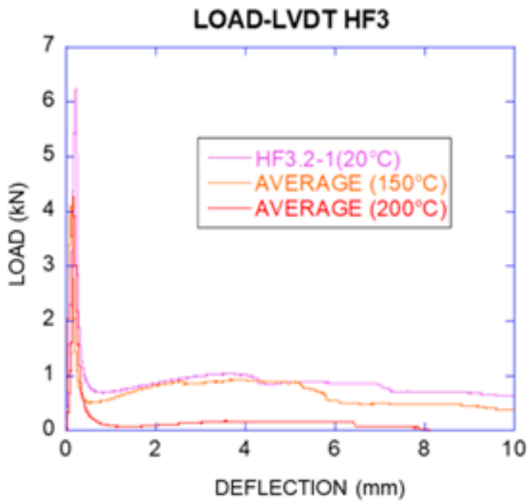


Figure 3: Load-load displacement curves of HF3 at various temperatures (average at each temperature) (Alberti, Gálvez, Enfedaque, & Castellanos 2021).

## 3 NUMERICAL SIMULATION

In this section the numerical work carried out to reproduce the experimental diagrams obtained for HF3 specimens is described. Firstly, the embedded cohesive crack model used to reproduce fracture is briefly described and, secondly, the finite element models are described. The description of the fracture model is very concise, since its development is not new, and the reader can find it in previous works (Sancho, Planas, Cendón, Reyes, & Gálvez 2007, Reyes, Gálvez, Casati, Cendón, Sancho, & Planas 2009, Gálvez, Planas, Sancho, Reyes, Cendón, & Casati 2013).

### 3.1 *Embedded cohesive crack model*

The cracking process is reproduced by means of the finite element method (FEM) by using an element formulation that takes advantage of the cohesive zone concept developed by Hillerborg (Hillerborg, Modéer, & Petersson 1976), inspired by the work of Dugdale (Dugdale 1960) and Barenblatt (Barenblatt 1962). This formulation constitutes a strong discontinuity approach proposed by Oliver (Oliver 1996a, Oliver

1996b) that was initially developed for concrete (Sancho, Planas, Cendón, Reyes, & Gálvez 2007, Gálvez, Planas, Sancho, Reyes, Cendón, & Casati 2013), but has also been successfully adapted for brickwork masonry (Reyes, Gálvez, Casati, Cendón, Sancho, & Planas 2009) and fibre-reinforced cementitious materials (Enfedaque, Alberti, Gálvez, & Domingo 2017). Since the cohesive zone approach assumes that fracture develops under mode I conditions, this approach considers that the cohesive stress vector $\boldsymbol{t}$ is perpendicular to the crack opening and parallel to the crack displacement vector $\boldsymbol{w}$:

$$\boldsymbol{t} = \frac{f(\tilde{w})}{\tilde{w}}\boldsymbol{w} \qquad \text{with } \tilde{w} = \max(|\boldsymbol{w}|) \tag{1}$$

where $f(|\tilde{w}|)$ stands for the material softening function, defined in terms of an equivalent crack opening $\tilde{w}$, which represents the maximum historical crack opening to account for possible unloading scenarios. In the case of PFRC, past works have proved that trilinear diagrams as shown in Figure 4 properly simulates fracture of this material with varying proportions of fibres, either with vibrated or self-compacting concrete, under mode I or a combination of mode I and mode II fracture conditions (Suárez, Gálvez, Enfedaque, & Alberti 2019) and correctly capturing fracture on different size specimens (Suárez, Gálvez, Alberti, & Enfedaque 2021). Unloading and reloading branches are aligned with the origin and the softening function is defined by four points ($t$, $k$, $r$ and $f$). The following expression provides the trilinear diagram shown in Figure 4:

$$\sigma = \begin{cases} f_{ct} + \left(\dfrac{\sigma_k - f_{ct}}{w_k}\right) \cdot w & \text{if } 0 < w \leq w_k \\ \sigma_k + \left(\dfrac{\sigma_r - \sigma_k}{w_r - w_k}\right) \cdot (w - w_k) & \text{if } w_k < w \leq w_r \\ \sigma_r + \left(\dfrac{-\sigma_r}{w_f - w_r}\right) \cdot (w - w_r) & \text{if } w_r < w \leq w_f \\ 0 & \text{if } w > w_f \end{cases} \tag{2}$$

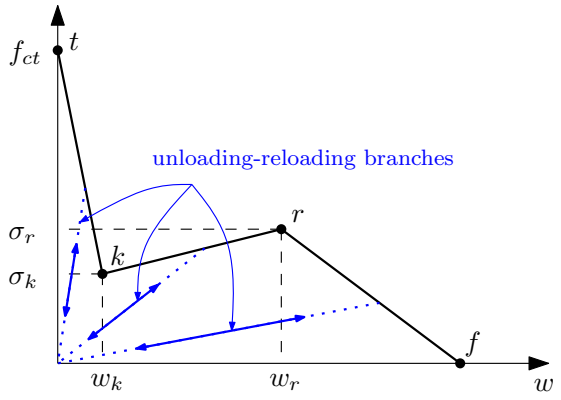


Figure 4: Scheme of the trilinear softening function used for modeling fracture of PFRC specimens.

This element formulation is programmed for constant strain triangular elements, thus accounting for an only integration point. Only three crack directions are considered, each of which are parallel to the triangle sides, and crack is placed at midheight; Figure 5 depicts these characteristics of the fracture model.

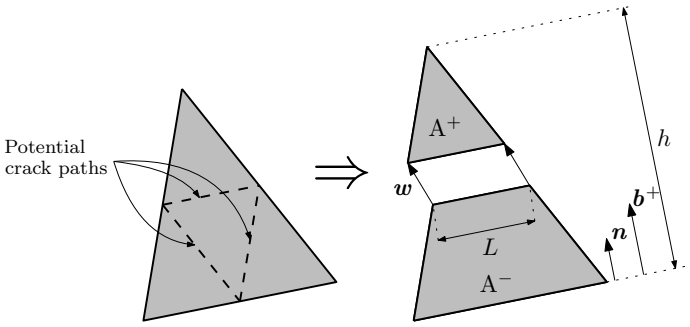


Figure 5: Embedded cohesive crack element.

Once the crack direction is determined, the element is divided into two parts, $A^+$ and $A^-$, and the stress vector $\boldsymbol{t}$, constant along the crack, can be obtained as:

$$\boldsymbol{t} = \frac{A}{hL}\boldsymbol{\sigma} \cdot \boldsymbol{n} \tag{3}$$

Where $A$ represents the area of the element, $h$ the triangle height over the side opposite to the solitary node, $L$ the crack length, $\boldsymbol{\sigma}$ the stress tensor and $\boldsymbol{n}$ the unit vector normal to that side and to the crack. Given that the crack is parallel to one side of the triangular element and is placed at midheight, (3) turns into $\boldsymbol{t} = \boldsymbol{\sigma} \cdot \boldsymbol{n}$. The reader can find a more detailed description of the model in (Sancho, Planas, Cendón, Reyes, & Gálvez 2007).

Inside the element, outside the crack the material remains elastic, thus the crack displacement vector $\boldsymbol{w}$ is solved assuming that the stress tensor can be obtained by subtracting an inelastic behaviour, which corrects the elastic prediction of the element by including the effect of the crack displacement, as expressed by (4).

$$\boldsymbol{\sigma} = \boldsymbol{E} : \left[\epsilon^a - \left(\boldsymbol{b}^+ \otimes \boldsymbol{w}\right)^S\right] \cdot \boldsymbol{n} \tag{4}$$

where $\boldsymbol{E}$ stands for the elastic tangent tensor, $\epsilon^a$ for the apparent strain vector obtained with the nodal displacements, $\boldsymbol{b}^+$ for the gradient vector corresponding to the solitary node, which in this case can be obtained with (5). Superscript $S$ denotes the symmetric part of the resulting tensor, : the double-dot product ($(\boldsymbol{A} : \boldsymbol{b})_{ij} = A_{ijkl}b_{kl}$), and $\otimes$ the direct product ($(\boldsymbol{a} \otimes \boldsymbol{b})_{ij} = a_i b_j$).

$$\boldsymbol{b}^+ = \frac{1}{h}\boldsymbol{n} \tag{5}$$

Given that $\boldsymbol{t} = \boldsymbol{\sigma} \cdot \boldsymbol{n}$ and by using expression (4) for $\boldsymbol{\sigma}$ and expression (3) for $\boldsymbol{t}$, the following expression is obtained:

$$\frac{f(\tilde{w})}{\tilde{w}}\boldsymbol{w} = [\boldsymbol{E} : \boldsymbol{\epsilon}^a] \cdot \boldsymbol{n} - \left[\boldsymbol{E} : \left(\boldsymbol{b}^+ \otimes \boldsymbol{w}\right)^S\right] \cdot \boldsymbol{n}$$

which can be rewritten as

$$\left[\frac{f(\tilde{w})}{\tilde{w}}\mathbf{1} + \boldsymbol{n} \cdot \boldsymbol{E} \cdot \boldsymbol{b}^+\right] \cdot \boldsymbol{w} = [\boldsymbol{E} : \boldsymbol{\epsilon}^a] \cdot \boldsymbol{n} \tag{6}$$

where $\mathbf{1}$ stands for the identity tensor. By means of an iterative algorithm (such as the Newton-Raphson method), the value of $\boldsymbol{w}$ can be computed to satisfy (6).

This model is implemented for ABAQUS® by means of an UMAT subroutine and, since vector $\boldsymbol{n}$, $\boldsymbol{b}^+$, crack length $L$ and the element area $A$ are computed with the nodal coordinates of each element, it reads an external file that stores this information.

### 3.2 *FEM models*

In order to reproduce the experimental results of (Alberti, Gálvez, Enfedaque, & Castellanos 2021), a bidimensional mesh, shown in Figure 6, has been used and plane stress conditions applied. This mesh is finer in the region where damage develops and coarser out of it, since only the vertical ligament above the notch is relevant in terms of the nonlinear problem to be solved. The adequacy of this refinement has been validated in previous works by the authors (Suárez, Gálvez, Enfedaque, & Alberti 2019, Suárez, Gálvez, Alberti, & Enfedaque 2021). The specimen size is 100 mm × 430 mm, supports are symmetrically placed at 300 mm from each other and loading is applied in the middle point of the upper side of the specimen, aligned with the notch, which is 33.3 mm long.

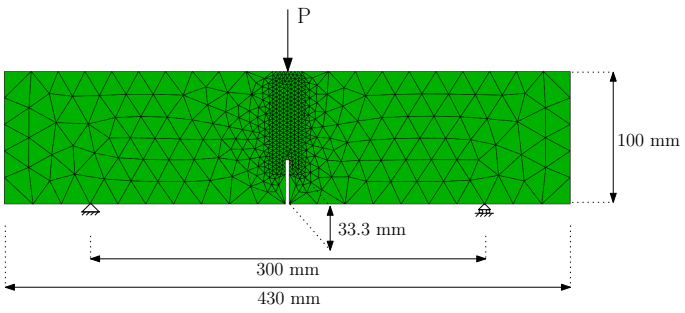


Figure 6: FEM model used in the numerical simulation.

## 4 RESULTS

In this section the results of the numerical simulations are presented, firstly introducing the trilinear softening diagrams used and, secondly, showing the load-deflection diagrams obtained, which are compared with the experimental results of (Alberti, Gálvez, Enfedaque, & Castellanos 2021).

### 4.1 *Trilinear softening diagrams*

The trilinear softening diagram is shown in Figure 4, the coordinates of four points must be fixed in the $\sigma$-$w$ plane, *t*, *k*, *r* and *f*. In order to use a coherent approach to define the coordinates of these points as temperature increases, the following criteria have been employed:

- **Point *t***. Due to the different elastic moduli of polyolefin and concrete, together with the negligible proportion of fibres in comparison with concrete, this point represents the tensile strength of concrete. This value is considered to reduce as concrete is subjected to higher temperatures, assuming a gradual degradation of the material.

- **Point *k***. This point represents the crack opening at which fibres begin to assume tensile stresses across the crack, thus reinforcing the material and producing a load recovery for subsequent load increments. This value has been obtained based on the softening diagram of a plain concrete, that is to say, without fibres. This simplification assumes that fibres contribution to the abscissa of this point is negligible, therefore the material follows the behaviour of a plain concrete.

- **Point *r***. The abscissa of this point, $w_r$, has been fixed with a value of 2.25 mm; this assumption is based on previous works by the authors (Suárez, Gálvez, Enfedaque, & Alberti 2019, Suárez, Gálvez, Alberti, & Enfedaque 2021). Regarding the value in the ordinate axis, $\sigma_r$, it has been considered to have the highest value at 20ºC and only equal or smaller values for higher temperatures have been contemplated. Since this parameter is related to the strength capacity of the fibres, it is assumed that higher temperatures can only degrade the material or the fibres surface, thus leading to equal or smaller values of $\sigma_r$.

- **Point *f***. This value is related to the fibre length and, following past results, a value of $w_f$=7.5 mm has been considered for all temperatures.

Following these criteria, the results that are presented in the following section are obtained with the trilinear softening diagrams shown in Figure 7 (the coordinates of these points for each trilinear diagram can be consulted in Table 3). It can be observed that $\sigma_k$ becomes lower as high temperature increases and $\sigma_r$ is remarkably similar for 20ºC and 150ºC, unlike in the case of 200ºC, for which it drops dramatically.

### 4.2 *Load-deflection diagrams*

Figure 8 shows the load-deflection diagrams obtained with the trilinear softening diagrams of Figure 7.

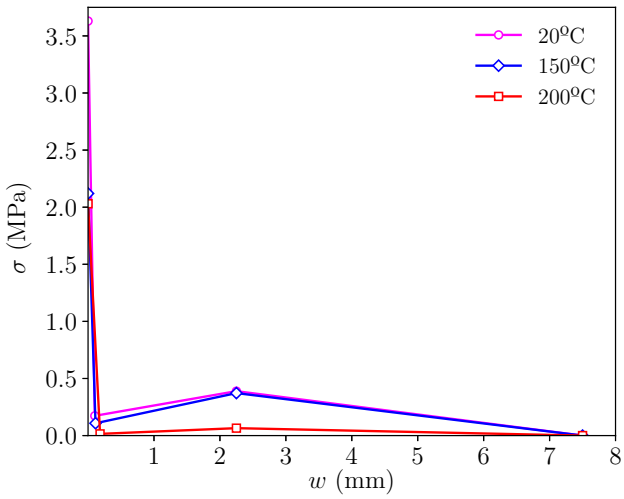


Figure 7: Trilinear softening diagrams used for simulating PFRC fracture specimens with a fibre proportion of 3 kg/m$^3$ subjected to different high-temperature conditions.

Table 3: Coordinates of *t*, *k*, *r* and *f* points of the trilinear softening diagrams shown in Figure 7.

| | 20ºC | 150ºC | 200ºC |
|---|---|---|---|
| $w_t$ | 0.000 | 0.000 | 0.000 |
| $\sigma_t$ | 3.630 | 2.120 | 2.030 |
| $w_k$ | 0.102 | 0.113 | 0.182 |
| $\sigma_k$ | 0.173 | 0.108 | 0.015 |
| $w_r$ | 2.250 | 2.250 | 2.250 |
| $\sigma_r$ | 0.389 | 0.372 | 0.065 |
| $w_f$ | 7.500 | 7.500 | 7.500 |
| $\sigma_f$ | 0.000 | 0.000 | 0.000 |

These results are presented with the same colours used in Figure 7 for each temperature and compare the numerical results, displayed in solid lines, with the experimental curves, in dotted lines.

In general, the initial peak load is well reproduced in all cases considering the inherent experimental scatter in this type of materials. The minimum load after the initial peak load is also very well captured, as well as the remnant peak load that takes place around $w = 4$ mm for all temperatures. In the case of 150ºC, the remnant peak load is numerically reproduced at an earlier value of $w$ if compared with the experimental result but in the authors' opinion this can be considered as valid, since only one experimental value for each temperature is available and, based on previous works, if a higher number of specimens had been tested for each case, the experimental envelopes would very likely cover the experimental results in all cases.

These results show that, up to temperatures below 200ºC, $\sigma_t$ and $\sigma_k$ decrease as temperature increases. This can be a consequence of moderate concrete and fibre degradation. Nevertheless, for temperatures below 200ºC, $\sigma_r$, which is responsible for the remnant peak load of PFRC, seems to be unaffected and a fixed value of 1.418 provides good numerical results for all temperatures below 200ºC. On the contrary, simulation of PFRC subjected to 200ºC requires a very different trilinear diagram that, not only requires lower values of $\sigma_t$ and $\sigma_k$, but a very low value of $\sigma_r$. This is a consequence of a high degradation of fibres at this temperature, that reduces their size, modifies their shape and their mechanical properties, as reported in (Alberti, Gálvez, Enfedaque, & Castellanos 2021).

## 5 FINAL COMMENTS

In this work, the numerical simulation of fracture of PFRC specimens exposed to high temperatures has been explored. To do this, some experimental results presented in (Alberti, Gálvez, Enfedaque, & Castellanos 2021) have been considered; the numerical results reproduce the behaviour of PFRC specimens manufactured with a fibre proportion of 3 kg/m$^3$ (HF3) and exposed to three temperatures: 20ºC, 150ºC and 200ºC. The numerical simulation of fracture has been carried out by means of a cohesive model fed with a trilinear softening function that had been successfully used in the past to reproduce the fracture behaviour of this material.

High temperatures modify the mechanical properties of polyolefin fibres, which results into variations of the softening diagram. The assumptions made to define the modified trilinear diagrams, described in section 4.1, have proved to be reasonable enough to correctly capture the main differences observed in the load-deflection diagrams induced by high temperatures. The softening diagram for a high-temperature

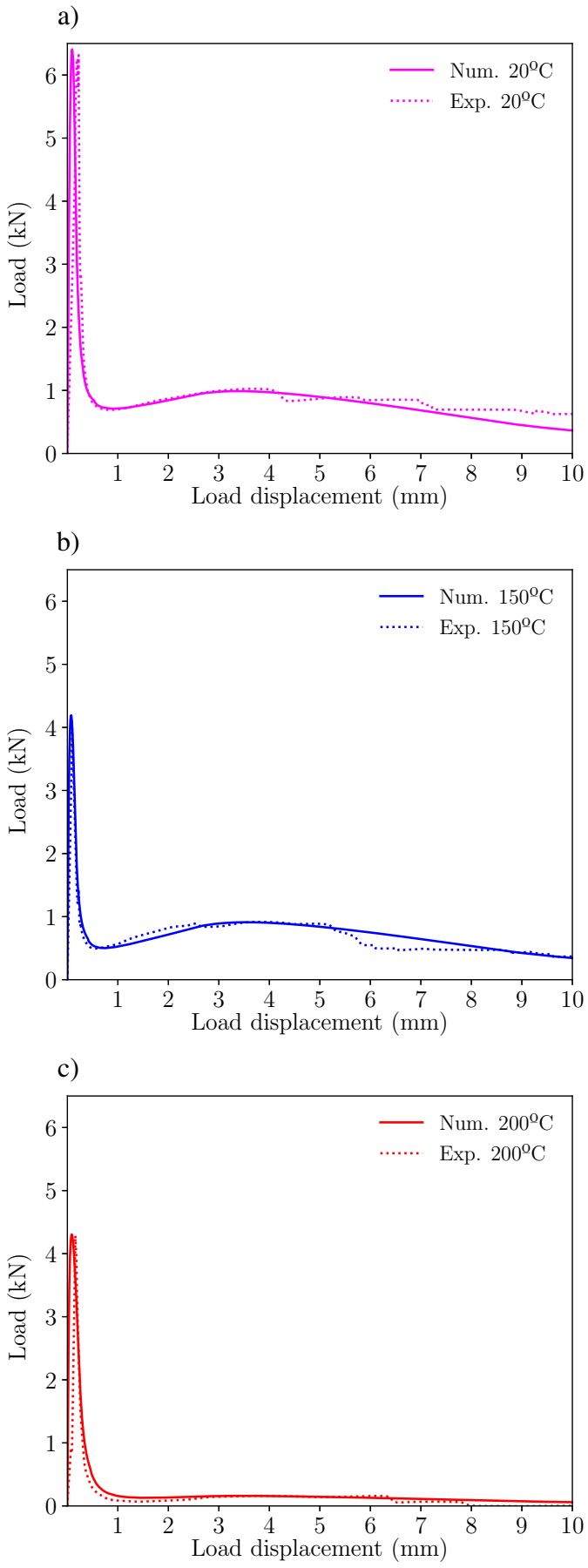


Figure 8: Comparison of load-deflection diagrams obtained numerically and experimentally for specimens of PFRC with 3 kg of fibres per $m^3$ subjected to different temperature conditions: a) 20ºC, b) 150ºC, and c) 200ºC.

exposure of 150ºC only presents slight modifications with respect to the ambient temperature of reference, 20ºC. On the contrary, the softening diagram corresponding to a high-temperature exposure of 200ºC has notable differences, remarkably reducing their reinforcing capacity. This is related to the severe degradation that polyolefin suffers at temperatures over 200ºC, which include a change of the fibre shape and modified mechanical properties of the material.

In (Alberti, Enfedaque, Gálvez, & Reyes 2017) the relation of the parameters of points $t$, $k$, $r$ and $f$ of the trilinear diagram (see Figure 4) with some measurable values and characteristics of the manufacturing of PFRC were explored and some expressions proposed with the aim of providing a predictive model of fracture for PFRC. The results presented in this work help to better understand how to numerically reproduce fracture of PFRC subjected to high temperatures, how to adapt the trilinear softening diagram when a cohesive model is employed and will hopefully help in providing a predictive fracture model of this material that also includes the effect of exposure to high temperatures. Nevertheless, this work only covers a limited number of temperature and an only fibre proportion (3 kg/$m^3$), and should be extended to a wider range of cases.

## ACKOWNLEDGEMENTS

The authors gratefully acknowledge the financial support provided for this research by the Ministry of Science and Innovation of Spain through the Research Fund Project PID2019-108978RB-C31.

## REFERENCES

Abdallah, S., M. Fan, & K. Cashell (2017). Pull-out behaviour of straight and hooked-end steel fibres under elevated temperatures. *Cement and Concrete Research 95*, 132–140.

Alberti, M., A. Enfedaque, J. Gálvez, & E. Reyes (2017). Numerical modelling of the fracture of polyolefin fibre reinforced concrete by using a cohesive fracture approach. *Composites Part B: Engineering 111*, 200–210.

Alberti, M. G. (2015). Polyolefin fibre-reinforced concrete: from material behaviour to numerical and design considerations. *Doctoral Thesis. Universidad Politécnica Madrid*.

Alberti, M. G., A. Enfedaque, & J. C. Gálvez (2015). Improving the reinforcement of polyolefin fiber reinforced concrete for infrastructure applications. *Fibers 3*(4), 504–522.

Alberti, M. G., A. Enfedaque, J. C. Gálvez, & L. Pinillos (2017). Structural cast-in-place application of polyolefin fiber–reinforced concrete in a water pipeline supporting elements. *Journal of Pipeline Systems Engineering and Practice 8*(4), 05017002.

Alberti, M. G., J. C. Gálvez, A. Enfedaque, & R. Castellanos (2021). Influence of high temperature on the fracture properties of polyolefin fibre reinforced concrete. *Materials 14*(3), 601.

Barenblatt, G. I. (1962). The mathematical theory of equilibrium cracks in brittle fracture. In *Advances in applied mechanics*, Volume 7, pp. 55–129. Elsevier.

Bažant, Z. P. & M. F. Kaplan (1996). Concrete at high temperatures: material properties and mathematical models.

Dugdale, D. S. (1960). Yielding of steel sheets containing slits. *J Mech Phys Solids 8*(2), 100–104.

Enfedaque, A., M. Alberti, J. Galvez, & M. Beltran (2018). Constitutive relationship of polyolefin fibre–reinforced concrete: Experimental and numerical approaches to tensile and flexural behaviour. *Fatigue & Fracture of Engineering Materials & Structures 41*(2), 358–373.

Enfedaque, A., M. Alberti, J. Gálvez, & J. Domingo (2017). Numerical simulation of the fracture behaviour of glass fibre reinforced cement. *Construction and Building Materials 136*, 108 – 117.

Enfedaque, A., M. G. Alberti, & J. C. Gálvez (2019). Influence of fiber distribution and orientation in the fracture behavior of polyolefin fiber-reinforced concrete. *Materials 12*(2), 220.

Gálvez, J., J. Planas, J. Sancho, E. Reyes, D. Cendón, & M. Casati (2013). An embedded cohesive crack model for finite element analysis of quasi-brittle materials. *Eng Fract Mech 109*, 369–386.

Hillerborg, A., M. Modéer, & P.-E. Petersson (1976). Analysis of crack formation and crack growth in concrete by means of fracture mechanics and finite elements. *Cem Concr Res 6*(6), 773 – 781.

Liu, X., G. Ye, G. De Schutter, Y. Yuan, & L. Taerwe (2008). On the mechanism of polypropylene fibres in preventing fire spalling in self-compacting and high-performance cement paste. *Cement and concrete research 38*(4), 487–499.

Lopez, J. A., P. Serna, E. Camacho, H. Coll, & J. Navarro-Gregori (2014). First ultra-high-performance fibre-reinforced concrete footbridge in spain: Design and construction. *Structural Engineering International 24*(1), 101–104.

Moradi, M., A. R. Bagherieh, & M. R. Esfahani (2020). Constitutive modeling of steel fiber-reinforced concrete. *International Journal of Damage Mechanics 29*(3), 388–412.

Oliver, J. (1996a). Modelling strong discontinuities in solid mechanics via strain softening constitutive equations. part 1: Fundamentals. *International journal for numerical methods in engineering 39*(21), 3575–3600.

Oliver, J. (1996b). Modelling strong discontinuities in solid mechanics via strain softening constitutive equations. part 2: Numerical simulation. *International journal for numerical methods in engineering 39*(21), 3601–3623.

Picazo, A., J. Gálvez, M. Alberti, & A. Enfedaque (2018). Assessment of the shear behaviour of polyolefin fibre reinforced concrete and verification by means of digital image correlation. *Construction and Building Materials 181*, 565–578.

Planas, J., G. Guinea, J. Gálvez, B. Sanz, & A. Fathy (2007). Indirect test for stress-crack opening curve, from experimental determination of the stress-crack opening curve for concrete in tension—final report of RILEM Technical Committee TC 187-SOC.

Reyes, E., J. Gálvez, M. Casati, D. Cendón, J. Sancho, & J. Planas (2009). An embedded cohesive crack model for finite element analysis of brickwork masonry fracture. *Engineering Fracture Mechanics 76*(12), 1930 – 1944.

Ruano, G., F. Isla, B. Luccioni, R. Zerbino, & G. Giaccio (2018). Steel fibers pull-out after exposure to high temperatures and its contribution to the residual mechanical behavior of high strength concrete. *Construction and Building Materials 163*, 571–585.

Sancho, J., J. Planas, D. Cendón, E. Reyes, & J. Gálvez (2007). An embedded crack model for finite element analysis of concrete fracture. *Engineering Fracture Mechanics 74*(1), 75 – 86. Fracture of Concrete Materials and Structures.

Suárez, F., J. Gálvez, A. Enfedaque, & M. Alberti (2019). Modelling fracture on polyolefin fibre reinforced concrete specimens subjected to mixed-mode loading. *Engineering Fracture Mechanics 211*, 244–253.

Suárez, F., J. C. Gálvez, M. G. Alberti, & A. Enfedaque (2021). Fracture and size effect of pfrc specimens simulated by using a trilinear softening diagram: A predictive approach. *Materials 14*(14).

Varona, F., F. J. Baeza, D. Bru, & S. Ivorra (2018a). Evolution of the bond strength between reinforcing steel and fibre reinforced concrete after high temperature exposure. *Construction and Building Materials 176*, 359–370.

Varona, F. B., F. J. Baeza, D. Bru, & S. Ivorra (2018b). Influence of high temperature on the mechanical properties of hybrid fibre reinforced normal and high strength concrete. *Construction and Building Materials 159*, 73–82.

Yermak, N., P. Pliya, A.-L. Beaucour, A. Simon, & A. Noumowé (2017). Influence of steel and/or polypropylene fibres on the behaviour of concrete at high temperature: Spalling, transfer and mechanical properties. *Construction and Building Materials 132*, 240–250.